

COMMUNICATION

Electrocatalytic H₂ evolution promoted by a bioinspired (N2S2)Ni(II) complex at low acid concentration

Received 00th January 20xx,
Accepted 00th January 20xx

Soumalya Sinha,^{a,#} Giang N. Tran,^{a,#} Hanah Na,^a and Liviu M. Mirica^{*a}

We have investigated a bioinspired (N2S2)Ni(II) electrocatalyst that produces H₂ from CF₃CO₂H with a turnover frequency (TOF) of ~200,000 s⁻¹ at low acid concentration (<0.043 M) in MeCN. We also propose an electrochemical mechanism for such an electrocatalyst toward H₂ production and benchmarked its activity by comparing its TOF and overpotential with those of other reported molecular Ni H₂ evolution electrocatalysts.

Hydrogen (H₂) is a key ingredient for fuel cell technologies needed for the future use of renewable energy sources on a larger scale.¹ The primary challenge of such technologies is to implement earth-abundant materials to produce H₂ with high turnover frequency (TOF) using mild acids. In this area, biological catalysts such as [NiFe] hydrogenases that exhibit TOFs of ~1000 sec⁻¹ under weak acidic conditions have been the inspiration for reducing H⁺ to H₂.^{2,3} The H⁺ transfer events are controlled at the Ni center, which is bound to two terminal cysteine (Cys) groups and two bridging Cys thiolates. The terminal in the HER catalytic cycle is the Ni-R state that releases H₂ and returns to the resting state Ni-Sla (Figure 1).⁴⁻⁶

Although structural mimics of [NiFe] hydrogenases have been reported, their performance in catalytic HER is either not described or kinetically sluggish.⁷⁻¹¹ Furthermore, there are other efficient mononuclear Ni complexes reported for electrocatalytic HER. For example, DuBois et al. reported Ni phosphine complexes that feature flexible amine arms as proton relay groups and perform HER using a strong acid, protonated dimethylformamide ([DMF-H]⁺, pK_a = 6.1 in MeCN).^{12,13} Dempsey et al. investigated the electrochemical HER mechanism of such Ni phosphine complexes and showed that the flexible second coordination sphere amine arms do not interact with the Ni center, yet they only shuttle protons

through H-bonding.¹⁴ However, a common drawback for these molecular HER electrocatalysts is the use of strong acids and often at high concentrations to achieve high turnover frequencies.

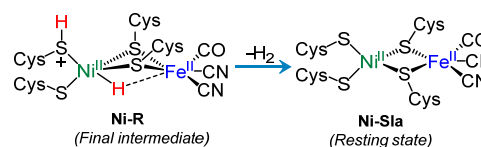


Figure 1. The final step observed in [NiFe] hydrogenases catalyzed the HER cycle.

A few reported molecular Ni^{II} electrocatalysts perform HER at low overpotential using weak acids. Jones and co-workers reported a S₂P₂-coordinated Ni HER electrocatalyst, which produces H₂ from CH₃CO₂H (AcOH, pK_a = 22.48 in THF) at only 240 mV of overpotential, yet with a low TOF of 1,240 s⁻¹.¹⁵ In addition, a Ni complex bearing phosphinopyridyl ligands with amine residues as H⁺ transfer sites showed comparatively higher TOF of 8,400 s⁻¹ using AcOH in MeCN (pK_a = 23.51), but at a high overpotential (590 mV).¹⁶

Herein we report the synthesis and characterization of a bioinspired Ni complex [(N2S2)Ni^{II}(MeCN)₂](OTf)₂, **1**·(OTf)₂, where N2S2 is 3,7-dithia-1,5(2,6)-dipyridinacyclooctaphane (Figure 2). We then studied the electrocatalytic HER reactivity of **1**²⁺ in MeCN using the acids CF₃CO₂H (TFA, pK_a = 12.65)¹⁷ or AcOH as the proton sources. Remarkably, **1**²⁺ showed a fast HER electrocatalytic activity with a maximum TOF of 195,000 s⁻¹ using only 0.043 M of TFA in MeCN with ≤2 M H₂O. We attribute such elevated performance of **1**²⁺ to the role pyridyl group of N2S2 in proton binding and transfer events during HER. Thus, the hemilabile¹⁸ nature of the pyridyl group in N2S2 that can act as both a ligand and a proton relay can be viewed as mimicking the role of Cys residues in [NiFe] hydrogenases.¹⁹

The N2S2 ligand was prepared following a slightly modified literature procedure,²⁰ and **1**·(OTf)₂ was synthesized as a purple solid in up to 90% yield.²¹ Single crystal X-ray analysis of **1**·(OTf)₂ reveals a tetragonally distorted octahedral coordination of the Ni^{II} center, with the two N atoms of the N2S2 ligand and two

^a Department of Chemistry
University of Illinois at Urbana Champaign
600 S. Mathews Avenue, Urbana, Illinois 61801.

* Email: mirica@illinois.edu

[#] These authors contributed equally.

Electronic Supplementary Information (ESI) available: [details of any supplementary information available should be included here].

MeCN molecules occupying the equatorial positions, with an average Ni–N bond distance of 2.06 Å (Figure 2). The two S atoms of N2S2 occupy the axial positions with comparatively longer average Ni–S bond lengths of 2.386 Å, thus completing a k^4 binding mode for the N2S2 ligand.

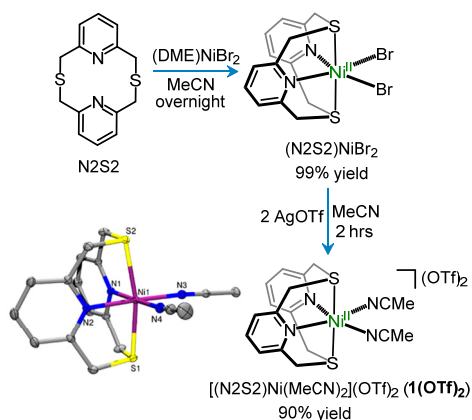


Figure 2. Synthetic scheme for $[(N2S2)Ni(MeCN)_2](OTf)_2$ (**1(OTf)₂**) and ORTEP representation (50% probability ellipsoids) for **1²⁺** (bottom left). Selected bond distances (Å): Ni1–N1 2.071(9), Ni1–N2 2.060(10), Ni1–S1 2.379(3), Ni1–S2 2.394(3), Ni1–N3 2.060(10), Ni1–N4 2.039(10).

We then studied the electrochemical behavior of **1²⁺** in N_2 -saturated 0.1 M nBu_4NPF_6 (TBAP)/MeCN. The cyclic voltammograms (CVs) of **1²⁺** showed a quasi-reversible redox wave centered at -1.30 V vs. $Fc^{+/0}$ and an irreversible wave at -1.75 V vs. $Fc^{+/0}$, assigned to the $Ni^{II/I}$ and $Ni^{I/0}$ redox couples, respectively (Figure 3).²¹ Scan rate dependence CVs confirmed diffusion-controlled electrochemical processes by exhibiting a linear correlation between the cathodic peak currents at the $Ni^{II/I}$ reductive wave and the square root of the scan rates (Figure S5 and S6).²²

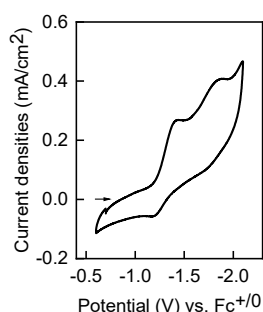


Figure 3. CV of **1²⁺** in N_2 -saturated 0.1 M TBAP/MeCN solution. Scan rate = 0.1 V/s.

The electrochemical HER activity of **1²⁺** was first tested using AcOH as the acid. The addition of AcOH showed an increase in the peak current densities at potentials lower than -2 V (Figure S7), yet the current enhancement for **1²⁺** overlapped with the background electrode contribution (Figure S11). A stronger acid, TFA, was then chosen, and the CVs recorded for **1²⁺** in the presence of TFA exhibit catalytic current enhancement for two cathodic peak potentials, $E_{pc}^{(1)}$ and $E_{pc}^{(2)}$, and the peak current densities increased as the concentration of TFA was increased up to 43.41 mM (Figure 4). The onset potentials of these

catalytic CVs were at least 500 mV more positive than the reduction potential of $Ni^{II/I}$, $E_{Ni^{II/I}}$. Additionally, the catalytic peak potentials (E_{cat}) were ≥ 365 mV more positive than that of GC-promoted HER in the absence of **1²⁺** (Figure S12).

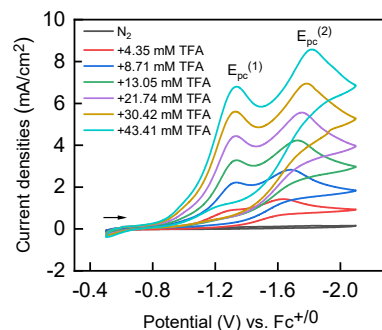


Figure 4. CVs of **1²⁺** (1 mM) without (black) and with different concentrations of TFA (4.35 mM – 43.41 mM) in N_2 -saturated 0.1 M TBAP/MeCN. $E_{pc}^{(1)}$ and $E_{pc}^{(2)}$ indicate the first and second cathodic peak potentials, respectively. Scan rate = 0.1 V/s.

To investigate the mechanism of HER process catalyzed by **1²⁺**, the shift in $E_{pc}^{(1)}$ was plotted vs. $\log[TFA]$ and fitted linearly to yield a slope of 23 mV/dec (Figure 5a, blue dots), indicating a typical EC-type electrochemical mechanism, where E is the Nernstian e^- transfer, followed by an irreversible chemical (C) step.²² The catalytic peak currents did not plateau upon the further increase in TFA concentration (>0.043 M), therefore the Randles-Sevcik equation cannot be applied. Instead, foot-of-the-wave analysis (FOWA) was used to estimate the apparent rate constants for the HER (k_{obs} , Table S1) by subtracting the background current due to HER performed by the bare GC electrode (Figure S16).¹⁷ The $\log(k_{obs})$ values were plotted vs. $\log[TFA]$ and a slope of 1.5 was obtained (Figure 5b), suggesting the order of the reaction in acid is greater than 1.

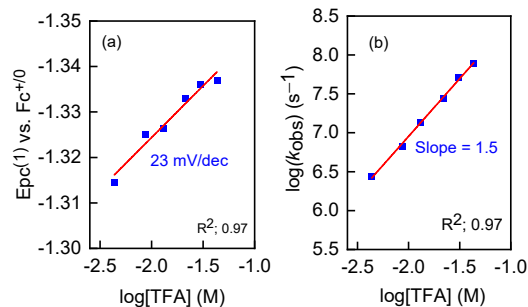


Figure 5. (a) Plot of first reductive peak potentials, $E_{pc}^{(1)}$ at different TFA conc. vs. logarithm of [TFA], 4.35 – 43.41 mM (blue dots). (b) Plot of the logarithm of k_{obs} obtained from FOWA vs. logarithm of [TFA] within the same concentration range as used in (a).

Based on these electrochemical results, we propose a catalytic HER mechanism in which **1²⁺** undergoes two sequential e^- reduction steps to generate the Ni^0 species **1** (Figure 6). The protonation (the C step) of **1** can generate **2**, which is tentatively assigned as a $(N2S2)Ni^{II}-H$ species. We propose that **2** adopts a square planar geometry where the non-chelating pyridyl group can get protonated or create a hydrogen bond with a TFA molecule, which may explain the greater than 1 order of the reaction in TFA. Furthermore, the protonation of the pyridyl

group in the following step could yield complex **3** that can release H₂ and regenerate **1**²⁺ upon solvation. Based on previous reports, the pK_a values for the pyridyl groups in pyridinophane ligands are between 5.75 and 6,²³ and thus it is expected that TFA could protonate a pyridyl group in N2S2 even in the presence of a metal ion. Thus, the pyridyl group the N2S2 ligand that is protonated in intermediate **3** could be viewed as mimicking the Cys residue in the Ni-R state of [NiFe] hydrogenase that can shuttle between a metal-bound state and a protonated state during the HER catalytic cycle.¹⁹

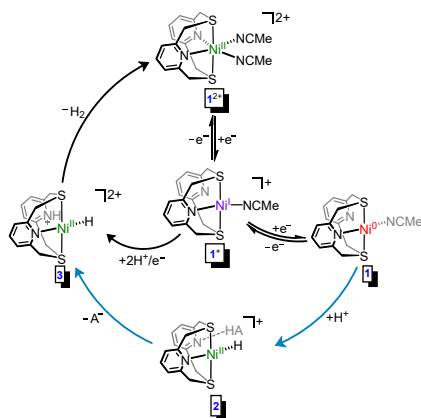


Figure 6. Proposed catalytic HER cycle (black arrows) for **1**²⁺. The blue arrows include the possible intermediate. HA = TFA.

To evaluate the effect of H₂O on HER catalysis, we employed a TFA concentration of 0.043 M in MeCN and three different H₂O concentrations (1.0 M, 1.5 M, and 2.0 M). Linear sweep voltammograms (LSVs) recorded for **1**²⁺ under these conditions show plateau currents at potentials lower than -1.75 V, and the shape of the LSVs remained unchanged as more H₂O was added (Figure 7).

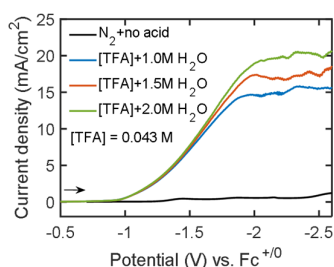


Figure 7. Linear sweep voltammograms for **1**²⁺ recorded in N₂-saturated 0.1 M TBAP/MeCN in the absence of TFA (blue) and the presence of 0.043 M TFA + different concentration of H₂O, 1 M (orange), 1.5 M (yellow), and 2.0 M (purple). Scan rate = 0.1 V/s.

FOWA was then carried out at the three different H₂O concentration and the average TOF_{max} determined for **1**²⁺ is 1.95 × 10⁵ s⁻¹ (Figure S18a and Table S2).²¹ Notably, the TOF_{max} values are independent of the H₂O concentration (Figure S18b), and thus the role of H₂O can be described as mainly impeding the homoconjugation of TFA in MeCN, without interfering with the thermodynamic parameters.¹⁷ The negligible effect on TOF_{max} upon the addition of more H₂O highlights the role of the pendant pyridyl group **3** toward HER. Overall, we posit that **3**

can produce H₂ as long as the pyridyl group of the N2S2 ligand is protonated, no matter how acidic the bulk electrolyte is.

The overpotential for the HER process was then calculated using the Appel and Helm method,²⁴ and found to be 730 mV at E_{cat/2} for **1**²⁺ in the presence of 0.043 M TFA with 1.5 M H₂O in MeCN. Under these conditions, chronoamperometric experiments carried out for **1**²⁺ showed a total charge of 200 mC passed over 15 mins of electrolysis at an applied potential of E_{cat/2}, corresponding to 1.03 × 10⁻⁶ moles of H₂ (Figure S13). Bulk electrolysis for **1**²⁺ was then performed at E_{cat/2} using a carbon cloth electrode to ensure formation of enough H₂, and 0.186 mmole of H₂ were detected by GC (Figure S15), corresponding to a Faradaic efficiency (FE) of 92%. While TFA is a comparatively a strong acid in MeCN, and bare carbon electrodes can perform HER using only TFA at potentials lower than -1 V,¹⁷ the average currents obtained for **1**²⁺ during bulk electrolysis were much higher than the background contribution (Figure S14). Although the background charge passed during the electrocatalytic HER process in the presence of the bare electrode is about 30% vs. the charge passed in the presence of **1**²⁺, the FE of the background HER process is low (< 25%) and does not contribute to more than 10% of the total H₂ produced (Figure S15).

To benchmark the HER activity of **1**²⁺, we selected five efficient Ni^{II}-based HER electrocatalysts, **4**,¹⁵ **5**²⁺,¹⁶ **6**²⁺,¹² **7**²⁺,¹³ and **8**²⁺ (Figure 9a).¹⁴ We have included the reported TOF values for these electrocatalysts and calculated the overpotentials by correcting the standard thermodynamic potentials (E_{HA}) for H⁺-to-H₂ conversion at the given pK_a of the acid (HA) used in the corresponding non-aqueous electrolyte (Eq. 1).¹⁷

$$E_{HA} = E^0 - (2.303RT/F) \times \text{p}K_a(\text{HA}); \quad \text{Eq. 1}$$

The logTOF values were then plotted vs. the calculated overpotentials (E⁰ - E_{HA}) for the Ni complexes mentioned above and **1**²⁺ (Figure 9b). Remarkably, **1**²⁺ performs electrocatalytic HER at a much higher TOF than those of **4**, **5**²⁺, **6**²⁺, and **7**²⁺. While the overpotential for **1**²⁺ is higher than most of these reported Ni complexes, it is comparable with that for **6**²⁺, albeit **6**²⁺ employs a strong acid, [(DMF)H]⁺, at concentrations >0.4 M. **1**²⁺ is also somewhat inferior to **8**²⁺ in terms of energetics, yet **8**²⁺ requires the use of ≤0.6 M of the stronger acid anilinium (pK_a = 10.62 in MeCN).^{14, 17} Overall, the electrochemical HER performance of **1**²⁺ is significant, especially since competitive HER kinetics can be achieved at low acid concentration using a weaker acid. By comparison, the only other Ni HER electrocatalysts containing thiolate and/or pyridine ligands, **4** and **5**²⁺, exhibit TOFs that are at least two orders of magnitude lower than that of **1**²⁺.

We also performed electron paramagnetic resonance (EPR) spectroscopy to detect a Ni^I species upon reducing **1**²⁺ with 1 equiv of CoCp*₂ (Cp* = pentamethylcyclopentadienyl). The X-band EPR spectrum in 1:3 MeCN:PrCN (v/v) at 77 K exhibited an EPR signal (Figure 10) that was simulated using a rhombic g tensor (g_x = 2.205, g_y = 2.152, g_z = 2.012). We attribute this EPR signal to a (N2S2)Ni^I species such as **1**⁺, suggesting a d_{x²-y²} ground state in a square planar geometry, and based also on the comparison with the EPR spectra of other reported Ni^I

complexes,^{25, 26} although the formation of a Ni^{III} species *in situ* via an oxidative process cannot be excluded.

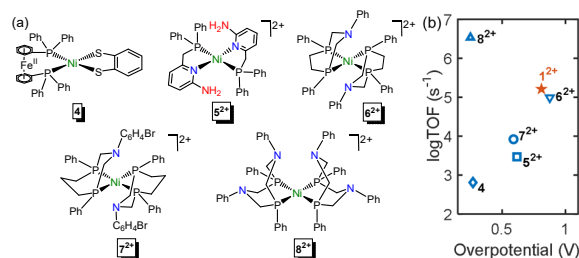


Figure 8. (a) Selected Ni^{II} HER electrocatalysts reported for efficient HER: **4**,¹⁵ **5**,¹⁶ **6**,¹² **7**,¹³ and **8**.¹⁴ The proton sources used are: 0.05 M AcOH in THF for **4**, 0.3 M AcOH in MeCN for **5**, 0.42 M [(DMF)H]⁺ + 1.2 M H₂O in MeCN for **6**, 1.26 M [(DMF)H]⁺ + 1.09 M H₂O in MeCN for **7**, and 0.6 M anilinium in MeCN for **8**. (b) Comparison of the logarithm of TOF vs. the calculated overpotential reported for the Ni electrocatalysts shown in (a) and **1**, the latter being in the presence of 0.043 M TFA + 1.5 M H₂O in MeCN.

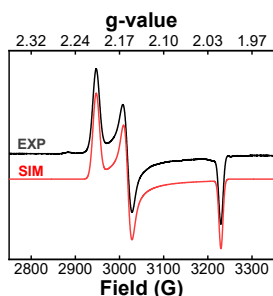


Figure 9. Experimental (black) and simulated (red) EPR spectra for **1**²⁺ after treating it with 1 equiv. of CoCp₂^{*} in 1:3 MeCN:PrCN glass at 77 K. The following g values were used for the simulation: g_x = 2.205, g_y = 2.152, g_z = 2.012.

In summary, we have synthesized and characterized a bioinspired complex [(N2S2)Ni(MeCN)₂]²⁺, **1**²⁺, that is an efficient HER electrocatalyst. This complex catalytically reduces protons to H₂ at low acid concentration. Given that most of the reported Ni-based molecular HER electrocatalysts perform HER using stronger acids than TFA, and often at high acid concentration,^{12–14} the performance of **1**²⁺ is remarkable as it achieves a high TOF for the HER. In addition, we highlight the role of the pendant pyridyl group of the N2S2 ligand in leading to elevated HER kinetics, which we consider resembles the proton-relay role of the Cys residue in [NiFe] hydrogenases that can also shuttle between a metal-bound and a protonated state. Although **1**²⁺ catalyzes the HER process at a high overpotential, 0.7 V, the proposed HER mechanism should inspire the development of improved bioinspired HER electrocatalysts that operate under benign reaction conditions.

We thank the Department of Energy's BES Catalysis Science Program (DE-SC0006862) for support of the initial work, and the National Science Foundation (CHE-1925751) for the support of the subsequent work. We thank Prof. Nigam P. Rath (Univ. of Missouri) for obtaining the crystal structure of **1**·(OTf)₂. We also thank the research facilities at the University of Illinois at Urbana-Champaign for their assistance.

Author Contributions

These authors contributed equally.

Conflicts of interest

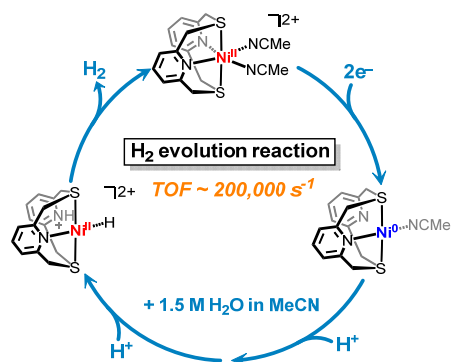
There are no conflicts to declare.

Notes and references

- N. S. Lewis and D. G. Nocera, *Proc. Nat. Acad. Sci. USA* 2006, **103**, 15729–15735.
- F. A. Armstrong, *Curr. Opin. Chem. Biol.*, 2004, **8**, 133–140.
- H. S. Shafaat, in *Comprehensive Coordination Chemistry III*, eds. E. C. Constable, G. Parkin and L. Que Jr, Elsevier, Oxford, 2021, pp. 707–730.
- W. Lubitz, H. Ogata, O. Rüdiger and E. Reijerse, *Chem. Rev.*, 2014, **114**, 4081–4148.
- R. D. Bethel and M. Y. Darensbourg, in *Bioorganometallic Chemistry*, 2014, pp. 239–272.
- T. Xu, D. Chen and X. Hu, *Coord. Chem. Rev.*, 2015, **303**, 32–41.
- A. Perra, E. S. Davies, J. R. Hyde, Q. Wang, J. McMaster and M. Schröder, *Chem. Comm.*, 2006, 1103–1105.
- Y. Ohki, K. Yasumura, K. Kuge, S. Tanino, M. Ando, Z. Li and K. Tatsumi, *Proc. Natl. Acad. Sci. U. S. A.*, 2008, **105**, 7652–7657.
- B. E. Barton, C. M. Whaley, T. B. Rauchfuss and D. L. Gray, *J. Am. Chem. Soc.*, 2009, **131**, 6942–6943.
- S. Canaguier, M. Field, Y. Oudart, J. Pécaut, M. Fontecave and V. Artero, *Chem. Comm.*, 2010, **46**, 5876–5878.
- M. E. Ahmed and A. Dey, *Curr. Opin. Electrochem.*, 2019, **15**, 155–164.
- M. L. Helm, M. P. Stewart, R. M. Bullock, M. R. DuBois and D. L. DuBois, *Science*, 2011, **333**, 863–866.
- S. Wiese, U. J. Kilgore, M.-H. Ho, S. Raugei, D. L. DuBois, R. M. Bullock and M. L. Helm, *ACS Catal.*, 2013, **3**, 2527–2535.
- E. S. Rountree and J. L. Dempsey, *J. Am. Chem. Soc.*, 2015, **137**, 13371–13380.
- L. Gan, T. L. Groy, P. Tarakeshwar, S. K. Mazinani, J. Shearer, V. Mujica and A. K. Jones, *J. Am. Chem. Soc.*, 2015, **137**, 1109–1115.
- R. Tamematsu, T. Inomata, T. Ozawa and H. Masuda, *Angew. Chem., Int. Ed.*, 2016, **55**, 5247–5250.
- B. D. McCarthy, D. J. Martin, E. S. Rountree, A. C. Ullman and J. L. Dempsey, *Inorg. Chem.*, 2014, **53**, 8350–8361.
- J. C. Jeffrey and T. B. Rauchfuss, *Inorg. Chem.*, 1979, **18**, 2658–2666.
- S. Ding, P. Ghosh, M. Y. Darensbourg and M. B. Hall, *Proc. Natl. Acad. Sci. U. S. A.*, 2017, **114**, E9775.
- T. Moriguchi, S. Kitamura, K. Sakata and A. Tsuge, *Polyhedron*, 2001, **20**, 2315–2320.
- See Supporting Information.
- A. J. Bard and L. R. Faulkner, *Electrochemical methods: Fundamentals and applications*, Wiley, 2001.
- W. D. Kim, D. C. Hrnir, G. E. Kiefer and A. D. Sherry, *Inorg. Chem.*, 1995, **34**, 2225–2232.
- A. M. Appel and M. L. Helm, *ACS Catal.*, 2014, **4**, 630–633.
- J. Y. Becker, J. B. Kerr, D. Pletcher and R. Rosas, *J. Electroanal. Chem. Interf. Electrochem.*, 1981, **117**, 87–99.
- M. Mohadjer Beromi, G. W. Brudvig, N. Hazari, H. M. C. Lant and B. Q. Mercado, *Angew. Chem., Int. Ed.*, 2019, **58**, 6094–6098.

COMMUNICATION

Table of contents graphic



We report a bioinspired (N₂S₂)Ni(II) complex that catalyzes the electrochemical H₂ evolution reaction (HER) with a turnover frequency (TOF) of $\sim 200,000 \text{ s}^{-1}$ at low acid concentration in acetonitrile.